Available online at www.sciencedirect.com

ScienceDirect

Current Opinion in
Colloid & Interface Science

Dynamic interfacial effects investigated by microfluidics: Formation and stability of droplets and bubbles

Boxin Deng and Karin Schroën

Abstract

Microfluidic techniques have emerged as powerful tools to unveil dynamic processes occurring during foam and emulsion production, and instabilities during their lifetime (coalescence and digestion), and to gain detailed insights in interfacial effects at (sub)millisecond time scales, including but not limited to, interfacial adsorption (i.e. dynamic interfacial/surface tension) and interfacial rheology. These insights are pivotal in connecting the interfacial effects to dynamic processes as they would occur during emulsion/foam production. We highlight the importance of conducting research at relevant time scales.

Addresses

Wageningen University, Laboratory of Food Process Engineering, Bornse Weilanden 9, 6708 WG, Wageningen, the Netherlands

Corresponding author: Deng, Boxin (boxin.deng@wur.nl)

Current Opinion in Colloid & Interface Science 2024, **73**:101826

This review comes from a themed issue on **Surface Analysis Techniques (2024)**

Edited by **Libero Liggieri** and **Reinhard Miller**

For a complete overview see the Issue and the Editorial

https://doi.org/10.1016/j.cocis.2024.101826

Keywords

Dynamic interfacial tension, Interfacial adsorption, Interfacial rheology, Coalescence, (sub) Milliseconds, Microfluidics, Partitioned-EDGE.

Introduction

Foams and emulsions are two-phase systems of which the stability amongst others is determined by the interfacial layer separating the phases and thus by the speed at which the layer is formed and stabilized. Destabilization processes, such as creaming, coalescence, and Oswald-ripening, occur simultaneously and synergistically across a broad range of time scales, and often also during production, ultimately leading to phase separation [1]. Product stability is typically monitored after production by macroscopic observation of, e.g. cream-layer height and microscopic observation of droplet size. When considering foam/emulsion stability at different length scales, as recently done by Wierenga, Basheva [2], it is important to realize that what happens at short times (during production) forms the basis for long-term development (after production), and these very short time scales are inherently difficult to capture and are often out of reach of current analysis techniques. In this review, we focus on microfluidic techniques to approach the time scales as they would occur during large-scale production. This would be for instance of 0.1−30 ms in high-pressure homogenizers and 0.1−1 s in colloid mills [3].

In microfluidic devices, micrometer-sized bubbles and droplets are typically formed at (sub)millisecond time scales, depending on the type of microfluidic device and the experimental conditions. Some devices have been upscaled (to certain extent) to prepare monodisperse emulsions [4], and some have been used as analytical tools to investigate, e.g. interfacial/surface tension and rheology [5,6] and coalescence behavior [7], initially to create fundamental insights, but more and more to serve as a link to practical applications. In this review, we discuss microfluidic tools used to capture interfacial phenomena and highlight the importance of capturing the underlying processes (during production) at relevant time scales.

Interfacial activity

Current understanding of interfacial behaviors

In Figure 1, we sketched a classical sequence of effects taking place during interface stabilization, which are 1) diffusion or convection from the bulk phase to the sub-interface layer; 2) diffusion through this 'imaginary' sub-interface layer to the actual interface; 3) adhesion to the interface; and 4) possible rearrangement at the interface (e.g. relevant for proteins) [8], e.g. leading to reduction of interfacial/surface tension in time. If the formation of an interfacial network takes place, this alters the rheological properties of the interface.

Depending on the emulsifier and process conditions used, a different reduction in interfacial/surface tension will occur, which is a consequence of the relative importance of the steps, as described in Figure 1. To put this into perspective, during foam and emulsion production, the characteristic time related to emulsifier adsorption needs to be considered relative to the

Figure 1

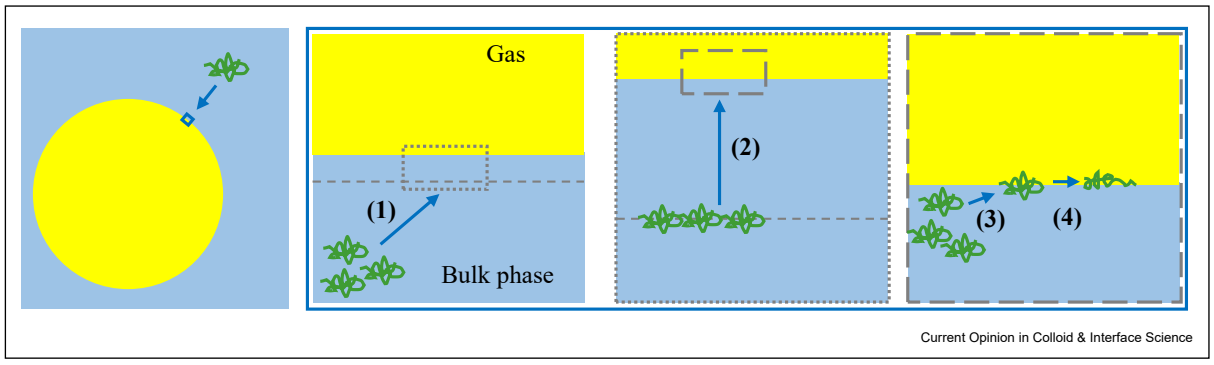

Schematic illustration of individual steps followed by emulsifier adsorption and rearrangement at the interface. Adapted from Ref. [9].

droplet/bubble formation time, which highly depends on the dispersion techniques (e.g. 0.1−30 ms in high-pressure homogenizers and 0.1−1 s in colloid mills [3]). When the characteristic adsorption time is three times shorter than the droplet formation time, the droplet size (without coalescence) is determined by the equilibrium interfacial tension [10,11]. Mostly, the characteristic adsorption time is comparable to or is longer than the droplet/bubble formation time, and the droplet size is a result of the dynamic effects related to adsorption and most probably to coalescence. It is crucial to understand the interfacial behavior of the selected emulsifier under process conditions as they would occur during product formation.

The steps described in Figure 1 are most frequently investigated using an automated drop tensiometer (ADT)—the so-called drop profile tensiometer for droplet and bubble surfaces, and also modeling has been used to understand interfacial composition and displacement as recently reviewed by Hinderink, Meinders [12]. Besides interfacial/surface tension, one can obtain insights about interfacial rheology by carrying out a series of expansions and compressions and using so-called Lissajous plots [13]. It is important to realize that ADT measurements are in the range of *seconds till hours*, or days when necessary, and at least 3 orders of magnitude slower than those encountered during emulsion and foam production.

During production, competing effects of droplet/bubble creation and interface stabilization against coalescence determine the droplet/bubble size of a newly made product. The question we are trying to address here is how we can connect these dynamic processes, and for that, only a limited number of techniques are available.

Short-term and long-term stability

Dynamic adsorption determines the creation and subsequent preservation of the newly created droplets/bubbles at short term. Popular techniques, such as the FoamScan, revolve around creating a foam and monitoring the height of the foam in time [14]. What is not taken into account is that the initial foam volume is likely the result of bubble formation and coalescence, and the decay in foam volume is the result of multiple destabilization processes, including coalescence and Oswald ripening [15]. To study dynamic processes at relevant length and time scales, highly dedicated tools are required—*microfluidics*. This is especially relevant for molecules that show complex interface behavior, such as proteins, that we shed light on in section 3.

Microfluidic techniques for droplets and bubbles

Microfluidic devices can be custom-designed to produce emulsions and foams, as well as to elucidate underlying interface mechanisms. Irrespective of the specific design of the microfluidic devices, the channel confinement largely guarantees the deformation and the subsequent break-up of the interface (i.e. droplet/bubble formation) and provides a precise control over emulsifier distribution in space and time [16]. Commonly used device geometries revolve around the use of shear or spontaneous droplet/bubble formation, as comprehensively reviewed by Refs. [17−19]. Each device has its pros and cons, concerning 1) the flexibility in tuning the droplet/bubble properties, 2) the feasibility for upscaling, 3) the system stability (e.g. against perturbations in applied pressures), and so on.

Microfluidics provide a broad range of configurations for the investigation of dynamic processes, including but not limited to, droplet/bubble formation (growth), interfacial adsorption (dynamic interfacial/surface tension), interfacial rearrangement, coalescence, and even digestion [20]. In this current opinion, we zoom in on the use of microfluidic tools to investigate the following: 1) the droplet/bubble formation cycle and underlying processes, 2) interfacial tension and rheology, and 3)

droplet/bubble coalescence. We wrap up with the utilization of microfluidic devices for sample preparation.

Dynamics of single droplet/bubble formation

Although the formation time is very short when investigated by microfluidics (e.g. (sub)milliseconds), one cycle of droplet/bubble formation can be further divided into substages [21−23]. To illustrate what is possible, we take the so-called partitioned-EDGE (with its full name as partitioned Edge-based Droplet GEneration) device as an illustrative example. In the partitioned-EDGE device, two deep channels are connected through a shallow area, which contains regularly separated pores that allow droplet and bubble formation to take place in the continuous phase (see Figure 2a). For bubble formation, it is regulated by two pressure regimes, which are divided by a transition pressure, namely the maximum Laplace pressure that directly correlates to the tension of an emulsifier-free interface. Bubble formation is dominated by dynamic adsorption and applied pressure in the first and second pressure regimes, respectively. The bubble formation time can be varied widely: 0.01−1000 ms, with one cycle of bubble formation being characterized by two substages (i.e. pore filling and necking stage), both of which possesses a typical time scale, namely the pore filling time and the necking time [23]. During the pore filling stage, the dispersed phase (re)fills the pore, and during the necking stage, the bubble volume (V_t) grows linearly (till V_0) as the neck width (w_t) reduces (from w_0) with time (Figure 2b). The bubble size (empty squares in Figure 2c) stays relatively constant within each pressure regime, while it rises up with increasing viscosity of the continuous phase (2−6 mPa•s), as shown in Figure 2d. When zooming in on the dynamics underlying the two substages, the bubble-volume growth rate is independent of the continuous phase viscosity (Figure 2e) that apparently slows down the thinning process of the neck (Figure 2f) and thus leads to larger bubbles [24]. These are all valuable and quantifiable insights that are also relevant for other microfluidic devices that were investigated for the production of emulsions and foams. To be complete, the formation of satellite droplets and bubbles, as observed at high concentrations of sodium dodecyl sulfate (SDS) (and whey protein isolate, WPI) (Figure 2g, inset in Figure 2h), allows shedding light on the flow pattern inside the pore and thus interpreting the role of continuous phase inflow during the necking stage (Figure 2h) [25].

Dynamic interfacial/surface tension and interfacial rearrangement

In many scaling relations used for emulsion and foam production, the interfacial/surface tension is used [27]. It is very important to use a realistic value rather than the value measured for clean or saturated interfaces [28]. However, that is more easily said than done since current methods such as the routine method ADT are not suited for use at high emulsifier concentrations and (sub)millisecond time scales (as was illustrated above). Besides, although it is well realized that reliable measurements with ADT are obtained with quiescent drop or bubble [29], the fact that emulsifier adsorption happens simultaneously during the creation of the pendant/rising drop or bubble, which often takes *a few seconds* depending on the experimental set-up and conditions, is rarely taken into account. This causes over interpretation of the adsorption dynamics, especially for fast-adsorbing emulsifiers. On the other hand, the maximum bubble pressure tensiometer (MBPT) has been used since decades as a complementary method to ADT for bubble system, to capture (dynamic) surface tension values at (sub)millisecond time scales (e.g. down to 10 ms [14], 1 ms [30], or even 0.1 ms [31], depending on the experimental set-up), yet it is important to note that the surface tension is captured during bubble growth, under the influence of hydrodynamic effects (i.e. inertia effects and aerodynamic resistance of the capillary). Moreover, corrections for dead time (to obtain the lifetime of the surface) and bubble deformation need to be considered, especially at short time scales. In this current opinion, microfluidic tensiometers (e.g. the partitioned-EDGE device) that are capable to access (sub)second time scales have been suggested for both droplets and bubbles as discussed next.

Microfluidic tensiometers

In literature, various devices for interfacial/surface tension measurement have been suggested that monitor I) the movement of a constricted interface inside a tapered capillary [32], II) the initiation of droplet formation after the Laplace pressure of the constricted interface is lowered below an externally applied pressure [6], III) droplet formation in the dripping regime using the size of droplets [33], IV) droplet formation in the transition and squeezing regimes (the so-called 'pressure-drop-based' measurement) [34], and V) deformation and droplet relaxation kinetics after formation in flow [35−37].

The partitioned-EDGE device uniquely allows measuring interfacial/surface tension as well as shedding light on coalescence stability during bubble formation. In the first pressure regime, the bubble size is almost independent of the applied pressures, from which the dynamic interfacial/surface tension *vs* time can be monitored as a function of the droplet/bubble formation frequency, and in the second pressure regime, there are data of the initial size of the bubbles (lower branch) and their eventual size after coalescence (top branch of the graph), see Figure 2c. In this section, the use of partitioned-EDGE device is illustrated, and we limit ourselves to interfacial/surface tension measurement. In

Figure 2

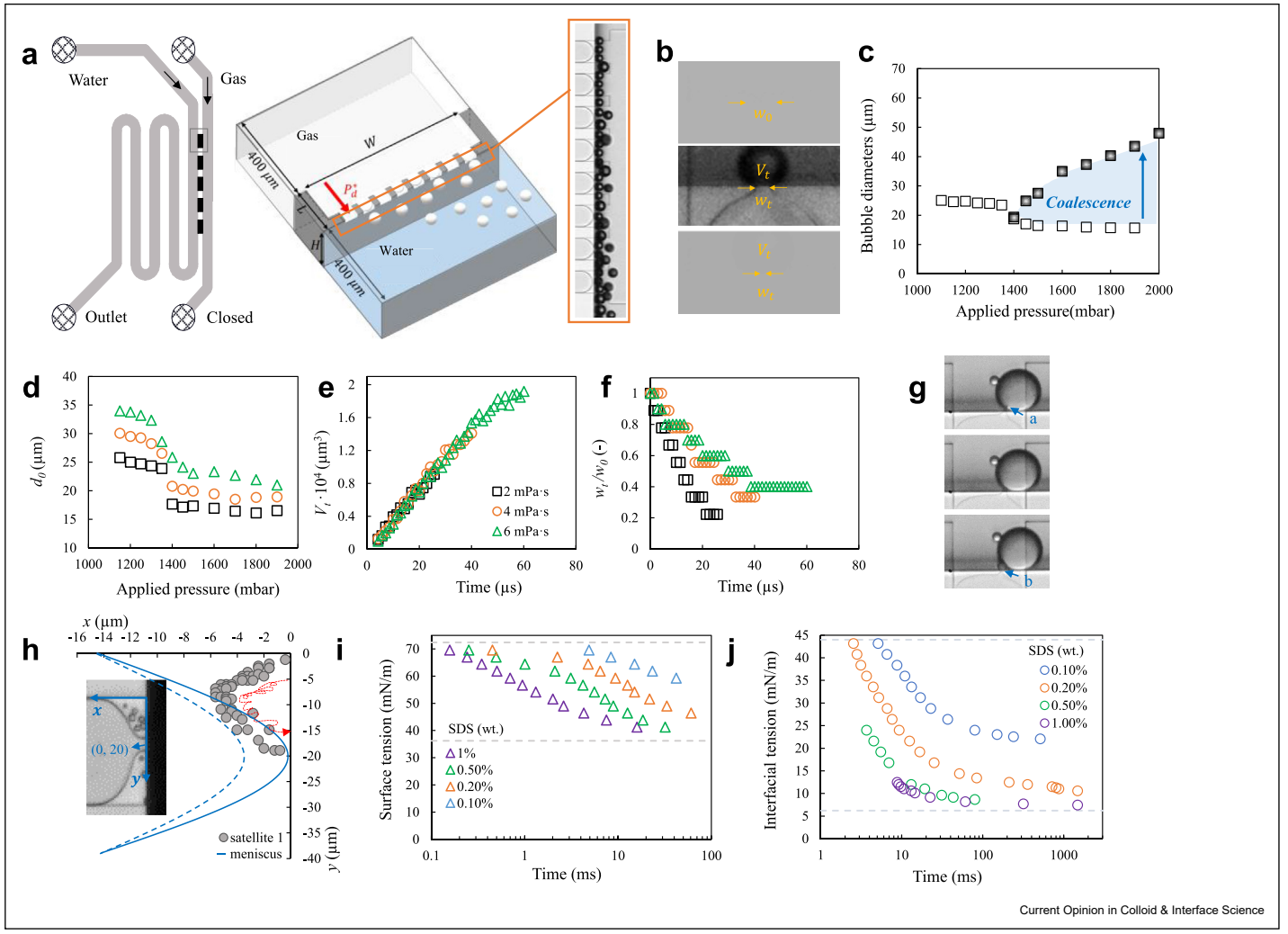

a. Layout of the partitioned-EDGE device, with the zoomed-in image showing bubble formation and coalescence at the pores. **b**. Microscopic images of the necking stage, showing the initial neck width (w_0), as well as the time-dependent neck width (w_t) and bubble volume (V_t). **c**. Bubble formation and coalescence as a function of the applied pressure in the partitioned-EDGE device. The initial and coalesced bubbles are represented by empty and filled squares, respectively. **d**. Initial size of bubbles as function of applied pressure for different viscosities of the continuous phase. Dynamic processes underlying the necking stage: bubble volume increasing irrespectively of viscosity (**e**) and neck-width thinning (**f**) with time as affected by viscosity. In **f**, the time-dependent neck width (w_t) is normalized to the initial value (w_0). In **c**, air and 5% wt. WPI, and in **d–f**, air and 2.5% wt. WPI were used as the dispersed and continuous phase, respectively, and the viscosity of WPI solutions was adjusted with glycerol. It is relevant to mention that as the viscosity varies in the range of 2–6 mPa•s, the weight percentage of glycerol in the 2.5% wt. WPI solution is at maximum 53.3%, and its potential impact on the mass transport of proteins is negligible, as proven by the unaffected bubble formation time in the first pressure regime where it is determined by dynamic adsorption [26]. **g**. The formation of satellite hexadecane droplet, snapping off at location a and then at location b, observed for 0.5% wt. SDS. **h**. The time-dependent location of one satellite bubble (gray symbols) inside the pore, with its trajectory (in- and out-movement inside the pore) indicated by the red arrow. The solid and dashed blue lines represent the location of the constricted meniscus when it is about to leap over the edge and when it just breaks up, respectively. **i–j**. Dynamic surface and interfacial tension as a function of the bubble/droplet formation time (at applied pressures below 1400 and 900 mbar, respectively) for the indicated SDS concentrations. Air and hexadecane were the dispersed phase in **i** and **j**, respectively. Figures are reprinted from Refs. [6,23–25] with permission from Royal Society of Chemistry and Elsevier. Abbreviations: SDS = sodium dodecyl sulfate; WPI = whey protein isolate.

the respective section 3.3, coalescence also will be discussed.

With the partitioned-EDGE device, the dynamic interfacial/surface tension *vs* time can be monitored in the absence of hydrodynamic effects related to flow of dispersed and continuous phase. Compared to MBPT, in which the surface tension is captured during bubble growth at the tip of a capillary, with the partitioned-EDGE device, the surface tension is derived for a *static* interface. Essentially, it revolves around a force balance across a *static* interface constricted inside the pore. The dynamic interfacial/surface tension achieved at the moment when the Laplace pressure of the constricted interface is reduced through dynamic adsorption to the externally applied pressure $\Delta P_{applied} = 2\gamma\left(\frac{1}{w}+\frac{1}{h}\right)\cos(\theta)$ can be calculated for a range of externally applied pressures that are limited by the minimum and maximum Laplace pressures that correspond to the interfacial/surface tension (γ) of a nearly saturated and clean interface, respectively. Here, it is important to point out that the dimensions (e.g. the height (h) and width (w) of the shallow pores) and the contact angle (θ) need to be known, and although the dimensions are customer-designed, the contact angle can be rather tricky to determine, especially when used under dynamic conditions. The corresponding time can be easily estimated by counting the number of droplets/bubbles formed (i.e. the droplet/bubble formation frequency), and relating that to the droplet/bubble formation time. It is relevant to mention that compared to MBPT, a 'dead time' also exists, and it is the time interval taken by the movement of the previously static interface to the pore exit and bubble growth. This time interval depends on phase properties (e.g. viscosity) and emulsifier properties, and for surface tension values shown in Figure 2i, it is less than 30 μs and thus negligible.

The accessible time scales in microfluidic tensiometers are mainly determined by the intrinsic characteristics of the microfluidic devices (e.g. dimension), the emulsifier properties, and the target interface. This differs from the routine methods of ADT and MBPT, with which they are limited by the measurement principles. With the partitioned-EDGE device, reduction in surface tension can be captured at >1.5 ms and >90 ms for 10% wt. and 1% wt. WPI, respectively, whereas at >0.1 ms and >5 ms for 1% wt. and 0.1% wt. SDS, respectively (Figure 2i). At comparable SDS concentrations (below and above the critical micellar concentration), the accessible time scales for reduction in interfacial tension are >1 ms with the 'EDGE tensiometer' (Figure 2j), >3 ms with the flow-focusing tensiometer [38], and 0.4–9.4 ms with the Y-junction tensiometer [33,39]. In a recently published work from our group, protein adsorption at high concentrations was investigated by EDGE tensiometer and ADT for both droplets and bubbles. These methods complement each other and show good agreement at intersecting time scales.

Depending on the microfluidic devices, image analysis is performed on one or a bunch of droplets (and bubbles) that are produced on-chip, which allows statistical evaluation of obtained values. Alternatively, image analysis of deformation of droplets that are produced off-chip has also been suggested [40]. It is relevant to mention that with EDGE tensiometer, although image acquisition is necessary, the interfacial/surface tension measurement is free of effects related to variations in droplet/bubble properties (e.g. shape and size) and the pixel resolution of the recording system. Moreover, pressure fluctuation measurement upon passage of slugs through a flow junction has been used [41]. Since the pressure measurement does not require visualization, it is expected to be especially of used for opaque products. For a comprehensive discussion, including the method-specific assumptions and technical limitations, we refer to a recent review by Kovalchuk and Simmons [42].

Irrespective of the device used and the type of interface, mostly, low–molecular weight surfactants (e.g. SDS) have been tested, and transport parameters (e.g. diffusion coefficient) have been derived for these components [32,34,36,38]. Microfluidic tensiometers have rarely been used for bubbles and complex emulsifiers such as proteins [25,43]. In principle, nothing is in the way of also exploring this, given the flight the field is taking, and that also includes, e.g. using higher temperatures, as demonstrated for coalescence [44].

Interfacial rheology

Using *the deformation and relaxation kinetics of droplets*, it is possible to monitor the process of interfacial adsorption and interfacial rearrangement. An example is the so-called 'Rheo-chip' (Figure 3a) [5]. Experimentally, the real-time droplet deformation (D; $D = (a-b)/(a+b)$, in which a and b are the drop dimensions that are perpendicular and parallel to the flow direction, respectively) are monitored. To obtain the interfacial tension, for example, Brosseau, Vrignon [36] proposed a scaling relationship $D_{max} = 0.8Ca^{2/3}R^{3.7}$ that describes the maximum deformation as function of the dimensionless capillary number Ca (e.g. $Ca = \frac{\mu_c \cdot v_d}{\gamma}$, where μ_c is continuous phase viscosity and v_d is droplet velocity) and a geometrical parameter (i.e. R—the droplet size that is regulated by device geometry and dimension).

When the interfacial layer exhibits rheological effects, the relaxation process is expected to follow an exponential decay of $D = D_{max} \cdot e^{\frac{-t}{\tau}}$, where t is the time and τ the characteristic relaxation time that is determined by the relative importance of elastic and viscous contributions. For proteins, a stretched exponential decay of $D = D_{max} \cdot e^{\frac{-t\beta}{\tau}}$ was used, which incorporates the

Figure 3

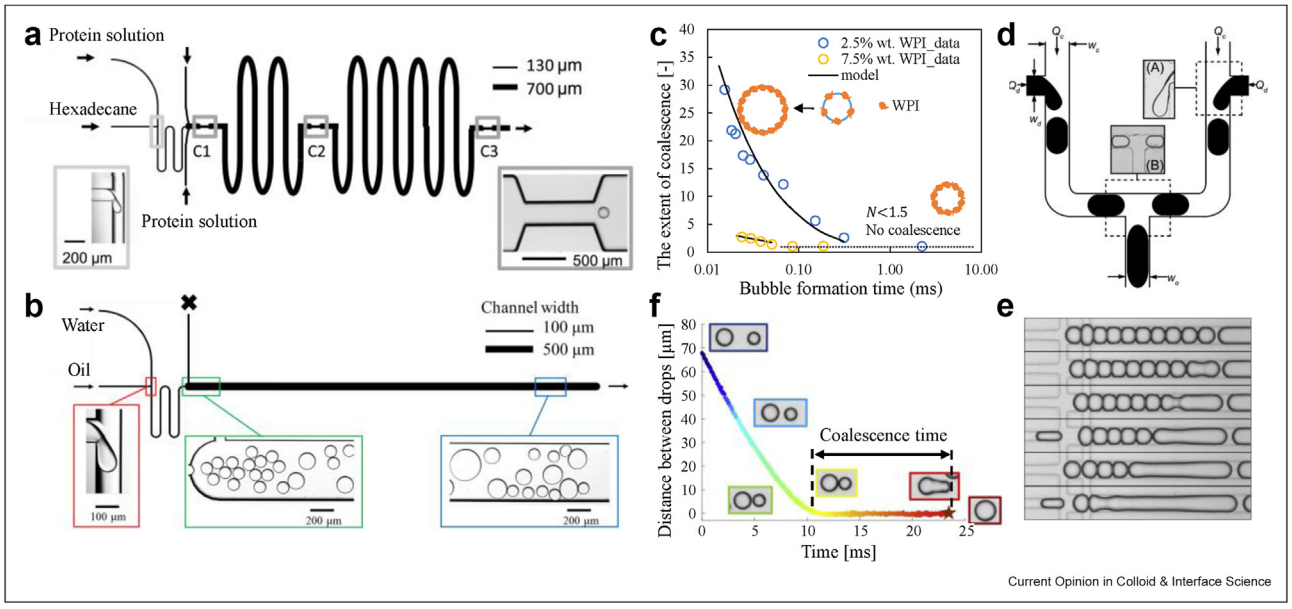

Layout of the Rheo-chip (**a**) and the coalescence cell (**b**). Adapted from Refs. [5,7], with permission from Elsevier. **c**. The extent of bubble coalescence, i.e. the number of coalescence events that a bubble with initial size has experienced, as a function of the bubble formation time; empty circles represent two experimentally obtained datasets, and the solid line represents the semiempirical model. Reprinted from Ref. [45], with permission from Elsevier. **d**. An example of coalescence phenomenon induced by device geometry: two bubbles are brought together to collide and coalesce at a T-junction; reprinted from Ref. [46], with permission from Royal Society of Chemistry. **e**. The cascade behavior of coalescence events; reprinted from Ref. [47] with permission from American Physical Society. **f**. The distance between two droplets in a coalescence events; reprinted from Ref. [48], with permission from Elsevier.

dynamically heterogenous nature of an protein-stabilized interface, with $\beta < 1$ indicating interfacial heterogeneity. Hinderink, de Ruiter [5] used the Rheo-chip to compare the interfacial behavior of whey protein isolate, pea protein isolate, and their blends at the liquid/liquid interface. Early-stage interfacial network formation (β in the range of 0.4–0.7) at (sub)second time scales (0.16–1 s) was found to occur. This is much faster than previously assumed to occur (i.e. ADT studies at time scales of hours), although it is still expected to be quite slower than the typical time scales needed for coalescence as will be discussed later. The importance of bringing comparable length and time scales together has been extensively discussed by Narayan, Metaxas [49], and for that, the use of microfluidics is a big step forward.

Coalescence stability

In emulsification and foaming processes, droplet/bubble formation (covered in the previous section) and coalescence occur simultaneously, which is directly reflected in the droplet/bubble size (i.e. larger) and size distribution. A coalescence event has three subprocesses, droplet approach leading to collision and droplet deformation, film drainage, and film rupture, as illustrated by Figure 4 [50]. To suppress coalescence, these individual stages need to be understood, and for this, microfluidic devices are useful tools. We first discuss microfluidic tools to quantify droplet/bubble coalescence in flow, and next, we focus on the subprocesses.

Droplet/bubble coalescence quantified by size measurement

In general, in microfluidic devices used to observe coalescence, variations in size of (originally monodisperse) droplets/bubbles are monitored. In the so-called 'coalescence cell' (Figure 3b), droplet/bubble formation and coalescence processes are decoupled. Monodisperse droplets (and bubbles) are formed upstream at a T-junction that is connected by a meandering channel to the coalescence observation chamber. The length of the meandering channel determines the adsorption time, which lies in the range of 11–173 ms for the device designs used by Muijlwijk, Colijn [7]. With an adsorption time of 100 ms, 0.005% wt. β-lactoglobulin is sufficient to stabilize hexadecane droplets very early on. Droplet coalescence has been investigated for different emulsifiers (type and concentration) [52–55] and process conditions such as temperature [44] and ionic strength [56], as well as highly concentrated emulsions [57].

Figure 4

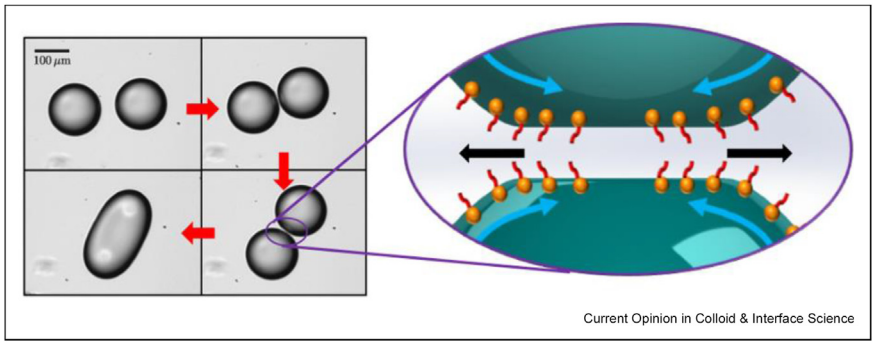

Images describing the processes of approaching, collision (accompanied by the drainage process of the liquid film), and merging of two droplets. The focus section on the right illustrates the fluid flow and the accompanied interfacial flow (Marangoni flow) during drainage. This picture is adopted from Narayan, Makhnenko [51], with permission from ACS Publication.

As mentioned in section 3.2, the partitioned-EDGE device can be used to study bubble coalescence [23]. Monodisperse bubbles are generated continuously and allowed to coalesce (with the bubble sitting in front of the pore, which is either an initial or a coalesced bubble) during or immediately after bubble formation. The extent of bubble coalescence is captured based on image analysis of bubble sizes (Figure 3c). Using this device, bubble coalescence has been monitored at time scales ranging from 0.01 to 3 ms, which is determined by the externally applied pressures and the device properties (i.e. design and dimension) for different types and concentrations of proteins [25] and continuous phase viscosities [45]. The extent of bubble coalescence is also captured in a semiempirical model based on a mass balance of proteins accumulating at the surface of the coalescing bubble (through coalescence and direct adsorption that expectedly follows a Langmuir isotherm). The experimental results and the model are in good agreement. Note that in this specific study, although protein adsorption at high concentrations (i.e. 2.5−10% wt. whey protein isolate) was examined, which limits the use of Langmuir isotherm [58], given the microsecond time scales encountered in the EDGE device and the measurement principle that bubble coalescence comes to a halt when the surface coverage is near-monolayer, the Langmuir isotherm was considered as a simple approach to describe interfacial accumulation (i.e. surface coverage) of protein molecules that have identical interfacial status, without too many additional effects playing a role, including but not limited to, the conformational states of protein molecules (e.g. molar area of adsorbed molecules; in other words, side or end-on adsorption of protein molecules [59]), protein unfolding, and intermolecular interactions between the adsorbed proteins at the interface, which are typically considered in advanced models [60,61] and expected to start playing a role at much longer time scales. Last but not least, it is also relevant to mention that to write such semiempirical models, diffusion coefficients as well as adsorption and desorption rate constants are needed but rarely available in literature.

To study bubble coalescence, the measurements with the coalescence cell and the partitioned-EDGE device can provide complementary information crossing a broad range of emulsifier concentrations and time scales. The coalescence cell is mostly used at low concentrations (e.g. 0.01−1% wt. β-lactoglobulin [52]), whereas the partitioned-EDGE device is used at high concentrations (e.g. 1−10% wt. whey protein isolate) [9]. The accessible range of time scales spreads across 4 orders of magnitude (e.g. 0.01−100 ms).

Droplet/bubble coalescence can also be intentionally and precisely regulated by device geometry as recently reviewed by Porto Santos, Cejas [62]. Generally, droplet/bubble pairs are brought together to collide (e.g. at a T-junction [46,63], Figure 3d, a trifurcating junction [64,65], and so on) and coalesce, with the extent of droplet/bubble coalescence depending on the experimental conditions (e.g. flow direction and speed). Bremond, Thiam [47] observed droplet coalescence taking place due to the formation of 'nipples' in the contact area that creates new surface area, leading to local depletion of surfactant molecules and thus coalescence. Based on this concept, the coalescence of a finite number of monodisperse droplets (with low concentrations of Span 80, or without surfactants) can be induced on-demand, following a cascade of coalescence events—the so-called *coalescence* '*avalanche*' (Figure 3e). Furthermore, Kovalchuk, Reichow [66] studied surfactant-laden and surfactant-free droplets forcing them to collide and coalesce at a T-junction. Driven by Marangoni effects, the surfactant-laden droplet wraps the surfactant-free droplet, with the merging rate being

proportional to the difference in interfacial tension between the droplets.

Collision and thinning

In the coalescence cell, different stages of a coalescence event (approach/collision, drainage, and rupture) can be distinguished. Krebs et al. and afterward Dudek performed extensive image analysis of the distance between drops and observed a linear decrease before a plateau phase (see Figure 3f). Two time scales have been defined, namely the contact time (i.e. the time during which the droplet/bubble pair stays in contact) and the drainage time (i.e. the coalescence time; the time necessary for the film to reach a critical thickness). The relative magnitude of these time scales allows to systematically and instrumentally investigate the impact of approach velocity, droplet/bubble size, dispersed phase fraction, dispersed and continuous phase viscosity, ionic strength, and emulsifier type and concentration on the propensity of droplet coalescence [48,56,67–69]. For example, it was found that both the contact and coalescence time are prolonged for larger droplets. They ascribed this to dimple formation and an increased volume of liquid film that needs to drain out. Moreover, based on initial work of Krebs, Dudek, Fernandes et al. [48] defined four regimes of droplet coalescence: 1) low-energy collision leading to minor deformation and coalescence; 2) bounce-off, so no coalescence; 3) high-energy collision with major deformation and coalescence; and 4) high-energy collision and splash. Furthermore, the droplet–droplet interactions transform from pair-wise to clusters, and eventually to close-packing as the volume fraction of the dispersed phase increases [70]. Building upon the understanding of different stages of one coalescence event, Williams, Wensveen [57] reported on the coalescence dynamics of multiple droplets using the so-called 'concentrate cell' (with its prototype being the coalescence cell) and found that the drainage time and thereby the coalescence stability increase with continuous phase viscosity before the compression force (that increases with the volume fraction) eventually outcompetes the impact of viscous dissipation. Compared to one-on-one coalescence, additional effects are relevant in a highly concentrated emulsion system, including but not limited to the assembling of droplets, droplet deformation, and droplet rearrangement, which further influence droplet coalescence during the lifetime of an emulsion product, yet were not well understood due to the none-transparency of emulsion products and technical limitations. Last but not least, the coalescence cell allows to investigate the temperature dependency of droplet coalescence and thus to generalize insights related to the importance of thermal waves that influence propensity of coalescence [44]. Moreover, droplet coalescence was investigated at enhanced gravity by placing a small microfluidic chamber on a centrifuge and investigating droplet deformation, which generated new insights in the critical disjoining pressure [71,72].

Upon collision, coalescence is influenced to certain extent by the mobility of the interface, with clean, mobile interfaces allowing for quick coalescence [73]. The mobility of an interface is a function of the physiochemical properties of the emulsifiers, and remains changing [49]. As the liquid film drains out from the contact area to the bulk phase, the flowing liquid causes a gradient in interfacial concentration, which suppresses coalescence by slowing down drainage (Marangoni effect). Besides the interfacial properties as discussed in former sections, in molecular dynamics simulations, it was shown that emulsifiers at high concentration slow down the coalescence process by inhibiting the formation of collective flow patterns inside droplets [74]. The combination of highly defined microfluidic experiments and high-resolution simulations is needed to make steps forward. For physical phenomenon–related drainage, including but not limited to interfacial transport and rheology, interested readers are referred to Ref. [75].

Production of well-defined droplets to elucidate other effects

Microfluidic devices have been used to produce monodisperse droplets, and efforts have been made to scale up these devices [4,76]. The partitioned-EDGE device allows to produce monodisperse droplets (with a coefficient of variation below 5%) with two sizes in two pressure regimes [4,77]. These emulsions have been used to quantitatively demonstrate the impact of droplet size on lipid oxidation with small droplets oxidizing faster than their larger counterparts mostly because of reaction kinetics for which the total surface area plays an important role [78]. In the so-called digestion on chip devices, the digestion of lipid droplets has been investigated by following the size of the droplet in time (Marze et al., 2014). This allows elucidation of the digestion kinetics at the level of droplets, which was a great step forward. Under *in vivo* conditions, droplet coalescence also occurs (which can also be quantified on chip [79]), leading to a reduction of total surface area available and thus of lipolysis. In this spirit, microfluidic platforms are useful tools for 1) high-throughput screening of formula and process conditions needed for the creation of functional emulsions, 2) pre-examining the digestion behavior of the functional emulsions under simulated gastrointestinal conditions, and finally, 3) predicting the digestion behavior of the functional emulsions under *in vivo* conditions.

Conclusions and outlook

In order to be in a position to predict product stability over its lifetime, effects taking pace at short time scales need to be considered. In this current opinion paper, we

have highlighted the use of microfluidics to assess short-term dynamic behaviors. As highlighted in section 3, the partitioned-EDGE microchip is multifunctional and allows both dynamic interfacial/surface tension and (bubble) coalescence investigation. The Rheo-chip allows capturing both (dynamic) interfacial/surface tension and early-stage formation of interfacial network (interfacial rheology). The dedicated devices for coalescence investigation (e.g. coalescence cell) allows both distinguishing different stages of one coalescence event and following the result of a series of coalescence events. We also see microfluidic techniques developing that are dedicated to tracking digestive behavior of emulsion droplets. These discussions provide a clear indication of using microfluidic tools for high-throughput screening of emulsifier properties and process conditions at short time scales.

It is important to keep in mind that for the development and application of microfluidic tools, opportunities and challenges coexist as recently reviewed by Schroen, Deng [20] from multiple aspects, including but not limited to the limit that microfluidic devices cannot mimic the turbulent conditions as encountered in industrial processes, which are expected to enhance interfacial adsorption and recoalescence, and the high level of demands for device production (e.g. device material, production technology, and post-treatment to optimize the geometrical and chemical feature of the microfluidic devices). Moreover, we want to point out that the *short-term dynamic behaviors* as highlighted in this opinion paper are expected to create the starting conditions for the *longer-term development* of an emulsion product; for instance, Oswald ripening (of foam) is more pronounced in a polydisperse system than in a monodisperse system, while they are not the only determining factors. The short-term coalescence behavior, as discussed in section 3.3, is mainly resulted from collisions in flow and differs from that typically described to occur after creaming and flocculation processes. Hence, when translating microfluidic insights to industrial processes and even to the lifetime development of emulsion (foam) products, additional processes that happen across a series of length and time scales need to be taken into account, and a direct translation is less appropriate.

To wrap up, we are convinced of the importance of understanding the dynamic behaviors at practically relevant (sub)millisecond time scales. We envision microfluidic devices as powerful tools that will allow for high-throughput screening of emulsifier properties as well as process conditions, all of which will contribute to the rational use of (existing or new-sourced) emulsifier materials and the optimum of production process of food emulsions and foams.

Declaration of competing interest

The authors declare that they have no known competing financial interests or personal relationships that could have appeared to influence the work reported in this paper.

Data availability

Data will be made available on request.

References

Papers of particular interest, published within the period of review, have been highlighted as:

* of special interest
** of outstanding interest

1. Tcholakova S, *et al.*: **Coalescence stability of emulsions containing globular milk proteins**. *Adv Colloid Interface Sci* 2006, **123–126**:259–293.

2. * Wierenga PA, Basheva ES, Delahaije RJBM: **Variations in foam collapse and thin film stability with constant interfacial and bulk properties**. *Adv Colloid Interface Sci* 2023, **312**, 102845.
This paper studied foam stability with a multiscale approach, and found that the foam instability is dominated by coalescence, which is further related to the properties of the liquid film rather than the interfacal properties.

3. Schultz S, *et al.*: **High-pressure homogenization as a process for emulsion formation**. *Chem Eng Technol* 2004, **27**:361–368.

4. Klooster St, Berton-Carabin C, Schroën K: **Design insights for upscaling spontaneous microfluidic emulsification devices based on behavior of the Upscaled Partitioned EDGE device**. *Food Res Int* 2022, **164**, 112365.

5. * Hinderink EBA, *et al.*: **Early film formation in protein-stabilised emulsions: insights from a microfluidic approach**. *Food Hydrocolloids* 2021, **118**.
This paper reported early-stage interfacial network at (sub)second time scales, in microfluidic devices. This is much faster than expected based on results obtained with the classical drop volume tensiometer.

6. * Deng B, *et al.*: **Capillary pressure-based measurement of dynamic interfacial tension in a spontaneous microfluidic sensor**. *Lab Chip* 2022, **22**:3860–3868.
This paper introduced EDGE as a versatile microfluidic device to investigate bubble formation and stability, and especially its use as microfluidic tensiometer for both droplets and bubbles.

7. Muijlwijk K, *et al.*: **Coalescence of protein-stabilised emulsions studied with microfluidics**. *Food Hydrocolloids* 2017, **70**:96–104.

8. Brösel S, Schubert H: **Investigations on the role of surfactants in mechanical emulsification using a high-pressure homogenizer with an orifice valve**. *Chem Eng Process* 1999, **38**: 533–540.

9. ** Deng B: **Microfluidic analysis of dynamic processes occurring during bubble formation and stabilisation**. In *Food process engineering*. the Netherlands: Wageningen Univeristy & Research; 2022.
A microfluidic study of dynamic processes underlying bubble formation and coalescence in the presence of proteins (whey protein isolate). The accessible time scales are in the range of 0.01–1000 ms, and similar to those found in industrial processes.

10. Wang K, *et al.*: **Mass-Transfer-controlled dynamic interfacial tension in microfluidic emulsification processes**. *Langmuir* 2016, **32**:3174–3185.

11. Kiratzis I, *et al.*: **Effect of surfactant addition and viscosity of the continuous phase on flow fields and kinetics of drop formation in a flow-focusing microfluidic device**. *Chem Eng Sci* 2022, **248**.

12. Hinderink EBA, *et al.*: **Interfacial protein-protein displacement at fluid interfaces**. *Adv Colloid Interface Sci* 2022, **305**, 102691.

13. Sagis LMC, Scholten E: **Complex interfaces in food: structure and mechanical properties**. *Trends Food Sci Technol* 2014, **37**: 59–71.

14. Shen P, *et al.*: **Cruciferin versus napin – air-water interface and foam stabilizing properties of rapeseed storage proteins**. *Food Hydrocolloids* 2023, **136**, 108300.

15. Wang J, Nguyen AV, Farrokhpay S: **A critical review of the growth, drainage and collapse of foams**. *Adv Colloid Interface Sci* 2016, **228**:55–70.

16. Whitesides GM: **The origins and the future of microfluidics**. *Nature* 2006, **442**:368–373.

17. Zhu P, Wang L: **Passive and active droplet generation with microfluidics: a review**. *Lab Chip* 2017, **17**:34–75.

18. Liu Z, *et al.*: **Advances in droplet-based microfluidic technology and its applications**. *Chin J Anal Chem* 2017, **45**:282–296.

19. Shang L, Cheng Y, Zhao Y: **Emerging droplet microfluidics**. *Chem Rev* 2017, **117**:7964–8040.

20. Schroen K, *et al.*: **Microfluidics-based observations to monitor dynamic processes occurring in food emulsions and foams**. *Curr Opin Food Sci* 2023, **50**.

21. Mi S, *et al.*: **Mechanism of bubble formation in step-emulsification devices**. *AIChE J* 2019, **66**.

22. Mittal N, *et al.*: **Dynamics of step-emulsification: from a single to a collection of emulsion droplet generators**. *Phys Fluids* 2014, **26**.

23. Deng B, Schroen K, de Ruiter J: **Effects of dynamic adsorption on bubble formation and coalescence in partitioned-EDGE devices**. *J Colloid Interface Sci* 2021, **602**:316–324.

24. Deng B, Schroen K, de Ruiter J: **Dynamics of bubble formation in spontaneous microfluidic devices: controlling dynamic adsorption via liquid phase properties**. *J Colloid Interface Sci* 2022, **622**:218–227.

25. Deng B, Schroën K, de Ruiter J: **A microfluidic study of bubble formation and coalescence tuned by dynamic adsorption of SDS and proteins**. *Food Hydrocolloids* 2023, **140**, 108663.

26. Deng B, Schroen K, de Ruiter J: **Dynamics of bubble formation in spontaneous microfluidic devices: controlling dynamic adsorption via liquid phase properties**. *J Colloid Interface Sci* 2022, **622**:218–227.

27. Rayner M, Dejmek P. In *Engineering aspects of food emulsification and homogenization*. Edited by Sun D, Boca Raton: CRC Press; 2015.

28. Schroën K, de Ruiter J, Berton-Carabin C: **The importance of interfacial tension in emulsification: connecting scaling relations used in large scale preparation with microfluidic measurement methods**. *ChemEngineering* 2020, **4**.

29. Javadi A, *et al.*: **Characterization methods for liquid interfacial layers**. *Eur Phys J* 2013, **222**:7–29.

30. Mucic N, *et al.*: **Dynamics of interfacial layers—experimental feasibilities of adsorption kinetics and dilational rheology**. *Adv Colloid Interface Sci* 2011, **168**:167–178.

31. Fainerman VB, *et al.*: **Dynamic surface tension of micellar solutions in the millisecond and submillisecond time range**. *J Colloid Interface Sci* 2006, **302**:40–46.

32. Kinoshita K, Parra E, Needham D: **Adsorption of ionic surfactants at microscopic air-water interfaces using the micropipette interfacial area-expansion method: measurement of the diffusion coefficient and renormalization of the mean ionic activity for SDS**. *J Colloid Interface Sci* 2017, **504**:765–779.

33. Muijlwijk K, *et al.*: **Interfacial tension measured at high expansion rates and within milliseconds using microfluidics**. *J Colloid Interface Sci* 2016, **470**:71–79.

34. * Liang X, *et al.*: **Determination of time-evolving interfacial tension and ionic surfactant adsorption kinetics in microfluidic droplet formation process**. *J Colloid Interface Sci* 2022, **617**:106–117.
This microfluidic study demonstrated the measurement of dynamic interfacial tension, and based on that derived surfactant kinetics (e.g., time-resolved surface concentration).

35. Hudson SD, *et al.*: **Microfluidic interfacial tensiometry**. *Appl Phys Lett* 2005, **87**, 081905.

36. Brosseau Q, Vrignon J, Baret JC: **Microfluidic dynamic interfacial tensiometry (μDIT)**. *Soft Matter* 2014, **10**:3066–3076.

37. Chen Y, Dutcher CS: **Size dependent droplet interfacial tension and surfactant transport in liquid-liquid systems, with applications in shipboard oily bilgewater emulsions**. *Soft Matter* 2020, **16**:2994–3004.

38. Kalli M, Chagot L, Angeli P: **Comparison of surfactant mass transfer with drop formation times from dynamic interfacial tension measurements in microchannels**. *J Colloid Interface Sci* 2022, **605**:204–213.

39. Santos TP, Deng B, Corstens M, Berton-Carabin C, Schroën K: **Interfacial protein adsorption behavior can be connected across a wide range of timescales using the microfluidic EDGE (Edge-based droplet GEneration) tensiometer**. *J Colloid Interf Sci* 2024, **674**:951–958.

40. D'Apolito R, *et al.*: **Measuring interfacial iension of emulsions in situ by microfluidics**. *Langmuir* 2018, **34**:4991–4997.

41. Xuan X, *et al.*: **A novel microfluidic method to simultaneously measure droplet size and interfacial tension without visualization**. *AIChE J* 2023, **69**, e18221.

42. ** Kovalchuk NM, Simmons MJH: **Review of the role of surfactant dynamics in drop microfluidics**. *Adv Colloid Interface Sci* 2023, **312**, 102844.
This review discussed surfactant dynamics and its influence on microfluidic processes and shed light on the application and limitations of microfluidic tools.

43. Guell C, *et al.*: **Apparent interfacial tension effects in protein stabilized emulsions prepared with microstructured systems**. *Membranes* 2017, **7**.

44. Bera B, Khazal R, Schroen K: **Coalescence dynamics in oil-in-water emulsions at elevated temperatures**. *Sci Rep* 2021, **11**, 10990.

45. Deng B, *et al.*: **Onsite coalescence behavior of whey protein-stabilized bubbles generated at parallel microscale pores: role of pore geometry and liquid phase properties**. *Food Hydrocolloids* 2023:138.

46. Christopher GF, *et al.*: **Coalescence and splitting of confined droplets at microfluidic junctions**. *Lab Chip* 2009, **9**: 1102–1109.

47. Bremond N, Thiam AR, Bibette J: **Decompressing emulsion droplets favors coalescence**. *Phys Rev Lett* 2008, **100**, 024501.

48. Dudek M, *et al.*: **Microfluidic method for determining drop-drop coalescence and contact times in flow**. *Colloids Surf A Physicochem Eng Asp* 2020:586.

49. Narayan S, *et al.*: **Zooming in on the role of surfactants in droplet coalescence at the macroscale and microscale**. *Curr Opin Colloid Interface Sci* 2020, **50**, 101385.

50. Chesters AK: **The modelling of coalescence processes in fluid-liquid dispersions: a review of current understanding**. *Chem Eng Res Des* 1991, **69**:259–270.

51. Narayan S, *et al.*: **Insights into the microscale coalescence behavior of surfactant-stabilized droplets using a microfluidic hydrodynamic trap**. *Langmuir* 2020, **36**:9827–9842.

52. Muijlwijk K: **Microfluidic methods to study emulsion formation**. In *Food process engineering*. the Netherlands: Wageningen University; 2017.

53. Baret JC, *et al.*: **Kinetic aspects of emulsion stabilization by surfactants: a microfluidic analysis**. *Langmuir* 2009, **25**:6088–6093.

54. Krebs T, Schroën K, Boom R: **Coalescence dynamics of surfactant-stabilized emulsions studied with microfluidics**. *Soft Matter* 2012, **8**.

55. Hinderink EBA, *et al.*: **Microfluidic investigation of the coalescence susceptibility of pea protein-stabilised emulsions: effect of protein oxidation level**. *Food Hydrocolloids* 2020, **102**.

56. Guo H, *et al.*: **Microfluidic investigation of the Ion-specific effect on bubble coalescencein salt solutions**. *Langmuir* 2023, **39**:8234–8243.

57. Williams YON, *et al.*: **Coalescence kinetics of high internal phase emulsions observed by a microfluidic technique**. *J Food Eng* 2024, **362**, 111739.

58. Lucassen-Reynders EH: **Competitive adsorption of emulsifiers 1. Theory for adsorption of small and large molecules**. *A: Physicochem Eng Asp* 1994, **91**:79–88.

59. Hunter JR, Kilpatrick PK, Carbonell RG: **Lysozyme adsorption at the air/water interface**. *J Colloid Interface Sci* 1994, **137**: 462–482.

60. Gochev GG, *et al.*: **β-Lactoglobulin adsorption layers at theWater/air surface: 5. Adsorption isotherm and equation of state revisited, impact of pH**. *Colloids Interf* 2021, **5**:1–26.

61. * Brigodiot C, *et al.*: **Studying surfactant mass transport through dynamic interfacial tension measurements: a review of the models, experiments, and the contribution of microfluidics**. *Adv Colloid Interface Sci* 2024, **331**:103239.
This review provided a comprehensive overview of (microfluidic) tensiometers and their usage to study surfactant mass transport.

62. Porto Santos T, Cejas CM, Cunha RL: **Microfluidics as a tool to assess and induce emulsion destabilization**. *Soft Matter* 2022, **18**:698–710.

63. Yang L, *et al.*: **Experimental study of microbubble coalescence in a T-junction microfluidic device**. *Microfluid Nanofluidics* 2011, **12**:715–722.

64. Zhou Q, *et al.*: **Investigation of droplet coalescence in nanoparticle suspensions by a microfluidic collision experiment**. *Soft Matter* 2016, **12**:1674–1682.

65. Tan Y-C, Ho YL, Lee AP: **Droplet coalescence by geometrically mediated flow in microfluidic channels**. *Microfluid Nanofluidics* 2007, **3**:495–499.

66. Kovalchuk NM, *et al.*: **Mass transfer accompanying coalescence of surfactant-laden and surfactant-free drop in a microfluidic channel**. *Langmuir* 2019, **35**:9184–9193.

67. Dudek M, Chicault J, Øye G: **Microfluidic investigation of crude oil droplet coalescence: effect of oil/water composition and droplet aging**. *Energy Fuel* 2019, **34**:5110–5120.

68. Krebs T, Schroen K, Boom R: **A microfluidic method to study demulsification kinetics**. *Lab Chip* 2012, **12**:1060–1070.

69. * Krebs T, Schroen K, Boom R: **Coalescence kinetics of oil-in-water emulsions studied with microfluidics**. *Fuel* 2013, **106**:327–334.
This study carried out high precision image analysis to obtain characteristic coalescence times, and provided a correlation between process conditions and emulsion stability.

70. Williams YON, Schroën K, Corstens MN: **A microfluidic method to systematically study droplet stability in highly concentrated emulsions**. *J Food Eng* 2023, **352**, 111535.

71. Feng H, *et al.*: **Manipulating and quantifying temperature-triggered coalescence with microcentrifugation**. *Lab Chip* 2015, **15**:188–194.

72. Krebs T, *et al.*: **Coalescence and compression in centrifuged emulsions studied with in situ optical microscopy**. *Soft Matter* 2013, **9**.

73. Liu B, *et al.*: **Coalescence or bounce? How surfactant adsorption in milliseconds affects bubble collision**. *J Phys Chem Lett* 2019, **10**:5662–5666.

74. Arbabi S, *et al.*: **Coalescence of surfactant-laden droplets**. *Phys Fluids* 2023, **35**, 063329.

75. Chatzigiannakis E, Jaensson N, Vermant J: **Thin liquid films: where hydrodynamics, capillarity, surface stresses and intermolecular forces meet**. *Curr Opin Colloid Interface Sci* 2021, **53**, 101441.

76. Schroën K, *et al.*: **Microfluidic emulsification devices: from micrometer insights to large-scale food emulsion production**. *Curr Opin Food Sci* 2015, **3**:33–40.

77. Sahin S, Schroen K: **Partitioned EDGE devices for high throughput production of monodisperse emulsion droplets with two distinct sizes**. *Lab Chip* 2015, **15**:2486–2495.

78. Klooster St: **Dynamics of lipid oxidation in emulsions across length scales**. In *Food process engineering*. the Netherlands: Wageningen University; 2023.

79. * Scheuble N, *et al.*: **Microfluidic technique for the simultaneous quantification of emulsion instabilities and lipid digestion kinetics**. *Anal Chem* 2017, **89**:9116–9123.
This microfluidic study visualized the digestion and coalescence of emulsion droplets under gastrointestinal conditions.